Available online at www.sciencedirect.com
ScienceDirect
Polymer 48 (2007) 4804–4813
polymer
www.elsevier.com/locate/polymer

Dense and square lattice-free colloid crystals of highly charged monodisperse latex particles on 3-aminopropyl trimethoxysilane-modified glass substrate

Jung Min Lee [a], Jung Hyun Kim [a], Chee Cheong Ho [b], In Woo Cheong [c,*]

[a] Department of Chemical Engineering, Yonsei University, 134 Shinchon-Dong, Sudaemoon-Ku, Seoul-120-749, Republic of Korea
[b] Faculty of Applied Sciences, Asian Institute of Medicine, Science and Technology, Amanjaya, 08000 Sungai Petani, Kedah, Malaysia
[c] Department of Applied Chemistry, Kyungpook National University, 1370 Sankyuk-dong, Buk-gu, Daegu 702-701, Republic of Korea

Received 30 October 2005; accepted 4 February 2007
Available online 14 June 2007

Abstract

Two- and three-dimensional colloid arrays are fabricated using highly charged, monodisperse poly(styrene/sodium *p*-styrene sulfonate) particles and 3-aminopropyl trimethoxysilane (APTMS)-modified glass substrates at 20 °C. The colloidal array patterns were investigated by SEM, AFM, and UV–visible analyses, and the pattern on the APTMS-modified glass substrate shows a denser packing and square lattice-free pattern without any crevices, as compared with that of cleaned, bare glass substrates. The adhesion force curves obtained from AFM analysis proved a negligible attractive force between APTMS and the poly(St/NaSS) particles. The APTMS layer guaranteed the free-slipping condition to prevent scattered pinnings of drawing particles into the nuclei. Consequently, the free-slipping led to a denser hexagonal close packing and particle deformation by a stronger capillary force arising from the reduced interstices among the particles. As a result, a dense (packing density ~ 0.80) fcc (or hcp) packing and narrower stop bands were obtained.

Keywords: Colloidal crystal; Deformation; Square lattice-free

1. Introduction

Colloidal particles have been used as the major components of industrial products, such as inks, coatings, paints, papers, cosmetics, and rheological fluids [1]. Recently, many researchers invented and studied novel materials based on colloidal particles, i.e., inorganic silica colloids and/or organic polymer latexes. Especially, photonic crystals for the visible range have been prepared by a self-assembly technique using polymer colloids of 100 nm in diameter, which are dried and crystallized into a face-centered cubic lattice [1–4]. In the current work, we focused on two-dimensional [5–9] and three-dimensional [10–13] (2- and 3-D) crystal structures from monodisperse polymer latex particles. Two- and three-dimensional periodic structures from monodisperse colloidal particles have become the focus of attention as versatile materials, such as microlenses, templates for optical filters, mesoporous membranes, photonic materials, sensors, and optical filters [1,10–18]. These structures can be easily prepared from the natural convection drying of latex under suitable conditions. In order to fabricate crystals of good quality onto a solid substrate, however, it is very important to understand the nature of colloidal particles and substrates and their interactions, as well as the nucleation mechanism of colloidal crystal [19–22]. The formation mechanism of crystals from latex particles on solid substrates was proposed by Nagayama et al. He demonstrated that the attractive capillary forces and the convective transport of particles toward an ordered region are the main factors governing a particle array [5]. A single crystal is usually isolated by large cracks, which originate from shrinkage during

* Corresponding author. Tel.: +82 53 950 7590; fax: +82 53 950 6594.
E-mail address: inwoo@knu.ac.kr (I.W. Cheong).

0032-3861/$ - see front matter © 2007 Elsevier Ltd. All rights reserved.
doi:10.1016/j.polymer.2007.02.071

the drying process. Each crystal possesses point defects, line defects, and dislocations, which are considered to be crystalline defects. In recent years, there have been numerous studies on the growth conditions of colloidal crystals, which are made by the convective drying method [5,11,23,24]. However, information on the packing density and array patterns of the crystals from the polymer particles is very limited [11,15,25–27].

In this study, we employed highly charged, monodisperse poly(styrene/sodium *p*-styrene sulfonate, St/NaSS) latex particles. 2- and 3-D particle arrays of these particles, formed by a natural convection drying method in an incubator at 20 °C, were applied on a hydrophobically modified glass substrate, which was prepared with 3-aminopropyl trimethoxysilane (APTMS) [28]. These were compared with those formed on a hydrophilic bare glass. Here, we proposed a facile method among the techniques that prevent scattered pinning of individual particles on a solid substrate, which causes defects of colloidal arrays.

2. Experimental section

2.1. Materials

Styrene monomer (St, Junsei, Japan) was purchased and purified using an inhibitor remover column (Aldrich, USA). The purified monomer was kept at −5 °C until use. Sodium *p*-styrene sulfonate (NaSS, Aldrich, USA) was purchased and used as received. Potassium persulfate (KPS, Junsei, Japan) was re-crystallized with methanol, dried in a vacuum oven, and kept at −5 °C until use. Sodium bicarbonate ($NaHCO_3$), 3-aminopropyl trimethoxysilane (APTMS), and anhydrous methanol were of analytical grade and used without further purification. Double-distilled and deionized (DDI) water was used throughout the experiment.

2.2. Preparation of highly charged, monodisperse poly(St/NaSS) latex particles

Highly charged, monodisperse poly(St/NaSS) latex particles were prepared by emulsifier-free emulsion polymerization with a two-stage shot-growth method [29,30]. In the first stage of polymerization, a small amount (0.24 mM) of NaSS was added to control the polydispersity and particle size. A second-stage shot of the monomer mixture (19.2 mM of styrene and 2.4 mM of NaSS) was injected at 90% conversion of the first stage polymerization. The prepared poly(St/NaSS) latex was purified using a serum replacement cell until the conductivity of the serum was the same as that of double-distilled and deionized water.

2.3. Preparation of the bare and APTMS-modified glass substrates

Glass microscope slides (Paul Marienfeld GmbH & Co.) were used as glass substrates (75 m × 25 mm with finely ground edges, pre-cleaned). The slides were cleaned in a 'piranha solution' (30% H_2O_2:98% H_2SO_4 = 1:3) at 120 °C for 1 h and then rinsed with distilled water, sonicated in methanol for 15 min, and dried under an N_2 atmosphere. In order to prepare the hydrophobic substrates, we modified the bare glass substrates with APTMS. The slides were dipped in a 2 wt% APTMS methanol solution for 30 min, rinsed with a 95% methanol aqueous solution and DDI water, dried by an N_2 flush, and then cured in a vacuum oven at 120 °C for 1 h.

2.4. Preparation of 2- and 3-D colloid crystal arrays

For 2- and 3-D colloid crystals, a natural convection drying method (~0.002 ml/h drying rate) was applied. The purified latex (0.02 wt% solid) was deposited on a stainless steel (40 mm × 40 mm × 2 mm) plate with a circular tapered hole (diameter = 15 mm, taper angle = 60°) in its center, and the cell was allowed to dry up in the incubator to form colloid crystals at 20 °C. Fig. 1a and b shows the cross-sectional view of a basic experimental cell and the schematic representation of the 2-D array formation from the monodisperse poly(St/NaSS) latex particles on the APTMS-coated glass substrate by the natural convective drying. A drop of the latex suspension with given volume and concentration was placed upon the substrate. The drop spread over the accessible glass area encircled by the stainless steel ring; the wall allowed water to be retained on its surface during drying due to the hydrophilicity of the stainless steel. The 60° tapered shape of the ring wall led to better wettability and maintained a concave air–water meniscus during drying of water. The magnet was used to avoid leakage from the latex suspension. A gap between the stainless steel ring and glass substrate was sealed with silicone grease to avoid leakage from the latex suspension.

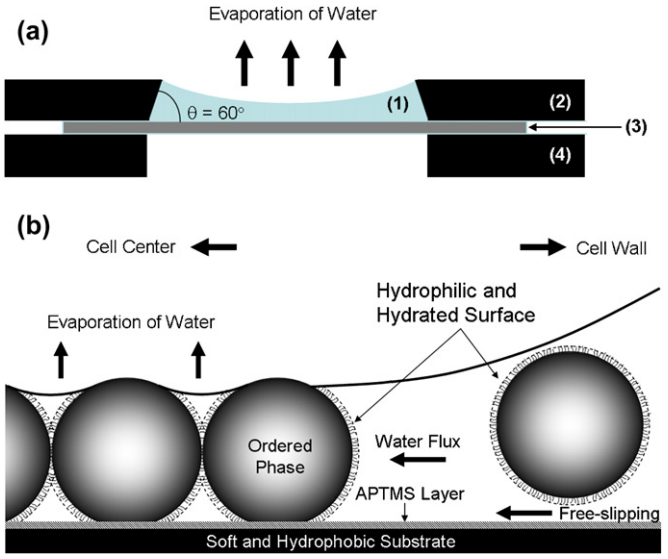

Fig. 1. (a) The cross-sectional view of a crystallization cell: (1) latex suspension, (2) stainless steel wall, (3) glass substrate, (4) circular magnet; and (b) the schematic representation of the 2-D array formation from monodisperse poly(St/NaSS) latex particles on the APTMS-coated glass substrate by natural convective drying.

3. Characterization

3.1. Particle size, particle size distribution, and surface charge density

The average particle size and polydispersity were determined by using a capillary hydrodynamic fractionation (CHDF-2000, Matec Applied Science, USA) and a field-emission electron scanning microscope (JSM-6500F, JEOL Co., Japan). The number-average particle size (D_n) and the polydispersity index (D_w/D_n) were 235 nm and 1.007, respectively. The surface charge density was measured by a titration method with 0.02 N NaOH aqueous solutions under an N_2 current. The surface charge density (σ) of the poly(St/NaSS) particle was 38 μC cm^{-2}.

3.2. Contact angle of the latex droplet on different substrates

Contact angles were measured by using a contact angle goniometer (SEO Phoenix 300, SEO Co., Korea). As shown in Fig. 2, the contact angles of the latex on the bare and APTMS-modified glass surfaces were 26° and 55° at 20 °C, respectively.

3.3. Drying rate of the latex on different substrates in the crystallization cell

Evaporation rates of the latex were measured by using a microbalance (LIBROR AEG-45SM, SHIMADZU, Japan). The average values with error bars obtained from 3 experiments are given in Fig. 3. As shown in Fig. 3, the evaporation rates of the latex in the crystallization cell on the bare and APTMS-modified glass surfaces at 20 °C were almost the same due to the same meniscus shape and the same area of a water–air interface. The hydrated and hairy particle surfaces were believed to retain water molecules and resulted in slow water evaporation, which ensured that the in-coming particles had enough time to fit into the pre-formed array pattern in the thin-wetting film. However, the changes of both evaporation rates were too similar to be discernible by using a balance.

3.4. Morphology of colloidal crystal pattern

Array patterns were observed by using a field-emission scanning electron microscope (FE-SEM, JSM-6500F, JEOL Co., Japan) and an atomic force microscope (AFM, Nanoscope III, Digital Instr., USA).

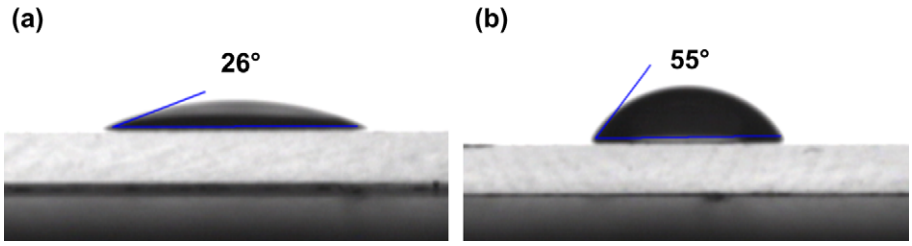

Fig. 2. Contact angle data of the 0.02 wt% poly(St/NaSS) latex droplets (a) on the cleaned, bare glass substrate and (b) on the APTMS-modified glass substrate.

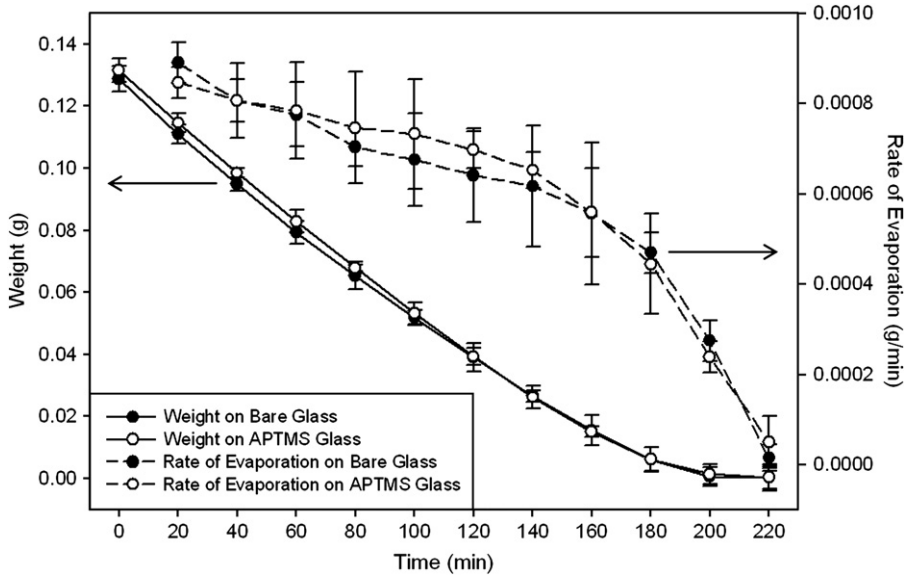

Fig. 3. Weight losses and evaporation rates of the latex particles in the crystallization cell on the bare and the APTMS-modified glass surfaces at 20 °C.

3.5. Packing density of colloidal crystal

The packing density of the crystal was obtained by using a UV–visible spectrophotometer (UV-1601PC, SHIMADZU Co., Japan). The UV–visible transmittance data of the crystal were obtained with a perpendicular incident light in the hexagonal close packing regions. The APTMS substrate showed reproducible and high quality spectrum in all points, but the spectrum from the bare substrate differed with a measuring spot, which was due to the different lattice structures between the hcp (or fcc) and square lattices.

3.6. Thickness of poly(styrene/NaSS) latex particles arrays

The thickness between the layers was determined by careful observation of an 85° tilted-view of an SEM image and the observed thickness between the layers was confirmed by using the following equations to avoid any possible error due to any hidden particles in-between the layers.

For a perfect hexagonal lattice,

$$\text{thickness} = d_o\left[1+\frac{\sqrt{2}}{\sqrt{3}}(N-1)\right]$$

For a perfect square lattice,

$$\text{thickness} = d_o\left[1+\frac{\sqrt{2}}{2}(N-1)\right]$$

where d_o is the original particle diameter and N is the number of layers.

4. Results and discussion

Fig. 4 shows the FE-SEM micrographs of the individual poly(St/NaSS) particles and the top-view of the multilayer arrays on the bare (a–c), and APTMS-modified (d–f) glass substrates at 20 °C. The crystal lattice of the bare glass substrate showed both tetragonal and hexagonal close packing (hcp or face-centered cubic, fcc) structures, but very few tetragonal structures (square lattices) were found in the APTMS-modified glass sample (b versus e). As can be seen in Fig. 4a, an individual particle lies on the bare glass substrate with no discernible deformation. On the other hand, the particles which adhered to the surface of the APTMS-modified glass substrate were clearly deformed as shown in Fig. 4d. The insets in Fig. 4a and d (the 85° tilted-view) provide further evidence on the adhesional deformation of the individual poly(St/NaSS) particle on the APTMS-modified glass substrate. In spite of the deformation, no substantial difference in the height of the individual particles on the bare glass (235.6 nm) and the APTMS-coated glass (236.3 nm) was observed.

A situation with the particle arrays on the APTMS-modified glass substrate is depicted in Fig. 1b. As water evaporated, a nucleus of ordered phase appeared when a cluster of particles forming the nucleus was partially immersed in a thin liquid layer on a horizontal substrate. When the particles were fully submerged in the water medium, strong electrostatic repulsions between the highly charged particles allowed the particles to maintain colloidal stability in the water medium during natural convection drying, even though the effective surface charge of the particles decreased during the drying process [31]. When the 'in-coming' particles by water flux toward the cell center were close to the nucleus, the lateral capillary force, formed at the water meniscus in the interstices between the hydrated poly(St/NaSS) particle surfaces, drew the particles by overcoming the weakened electrostatic repulsion between the particles.

For a close packing, the in-coming particles should move freely and closely attach to the pre-formed nuclei. 'Free-slipping' is important in ensuring formation of a defect-free colloidal crystal, since scattered anchorings of individual particles on the glass substrate cause defects as Nagayama et al. mentioned that the crystal defects originated from the pinning of particles on the glass substrate [5]. To clarify the fact that the APTMS layer provided the free-slipping condition, we measured indirectly (i.e., not in the wet state) the attractive force between the surface of the latex particles and the APTMS layer by using an AFM, as shown in Fig. 5. It was found that the attractive force between the APTMS-modified SiN_x AFM tip and the surface of the latex particles was negligible as compared with that of an SiN_x AFM tip. The adhesion force values of the latex particles surface–SiN_x AFM tip and surface–APTMS-modified SiN_x AFM tip were -19.1×10^{-10} N and ~0 N, respectively. Even though we could not measure directly the attractive force between the surface of the latex particles and the APTMS layer, one can estimate that the measured attractive force values are pertinent, since the difference of van der Waals attraction force between in air and in water is about one order, obtained by using Hamaker constants. From this result, we concluded that there was no substantial adhesion between the latex particle surface and the APTMS-modified SiO_2 substrate in the wet state.

If a moving particle came to stop and weighed on the 'grass-like' soft substrate, the contact surface of the substrate deformed to close up the surface of the particle. The APTMS coating seemed to offer a softer substrate surface, like ''grass'', than the bare glass substrate, thus providing a greater contact area of poly(St/NaSS) particles with the APTMS coating. As a result of the greater contact area, the interstice between the particle and the APTMS surface was reduced. This reduced interstice provides a stronger capillary force (by Young–Laplace equation), and this larger capillary force at the water meniscus in the interstices caused the adhesional deformation of the hydrated particles during natural convection drying [32]. The 'in-coming' particles on the APTMS layer easily attached closely to the nuclei without anchoring onto the peripheral surface, and then the adhesional deformation occurred as water evaporated. In other words, the free-slipping condition made dense packing favorable which enabled the adhesional deformation by means of the reduced

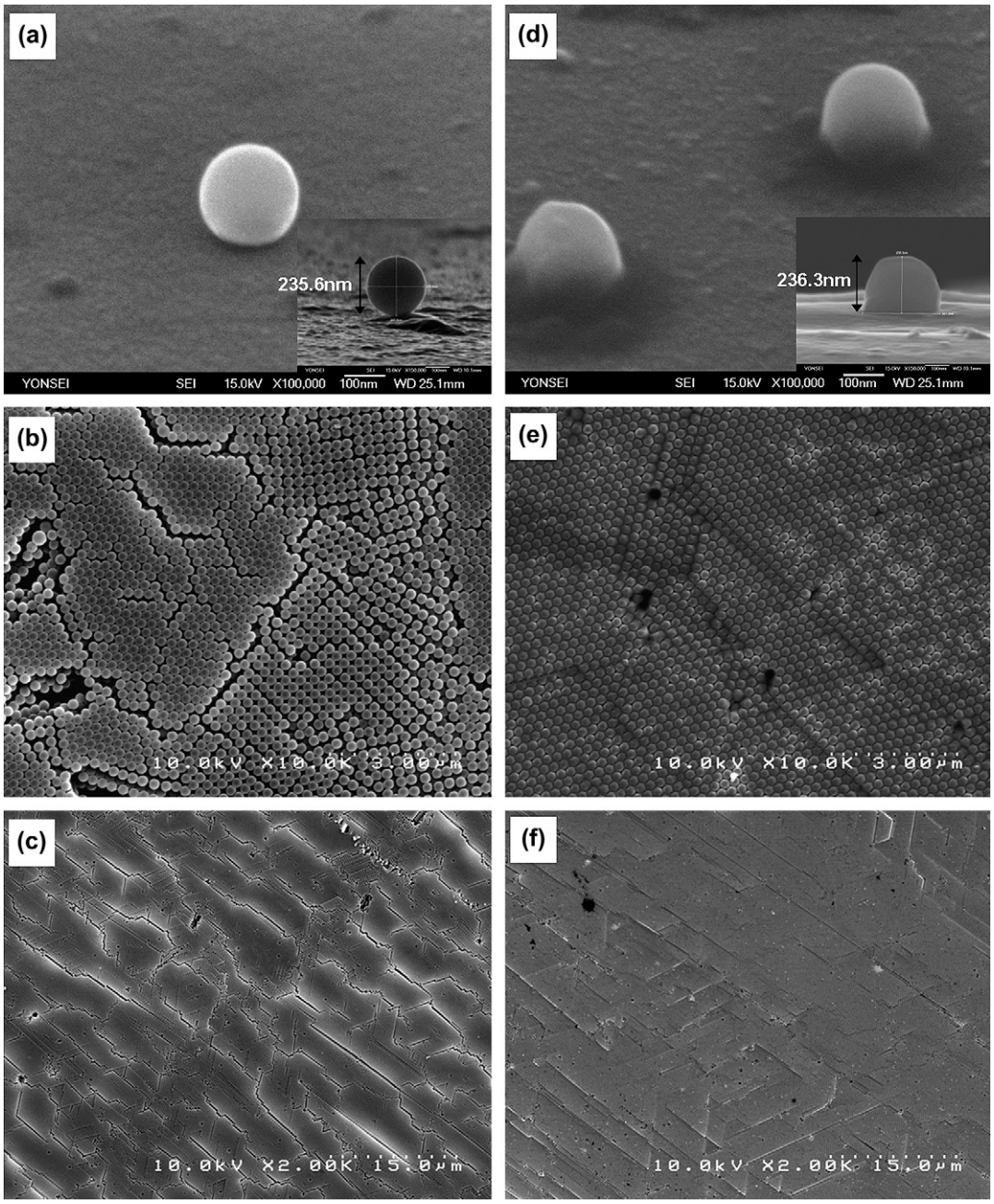

Fig. 4. FE-SEM photos of 234 nm highly charged poly(St/NaSS) particles: (a) and (d) 60° tilted-view of individual particles (insets: 85° tilted-view), (b) and (e) top-view of multilayer at high magnification (×10,000), (c) and (f) top-view of multilayer at low magnification (×2000); (a)–(c) on the cleaned, bare glass substrate and (d)–(f) on the APTMS-modified glass substrate at 20 °C.

interstices between particle and particle or between particle and surface of the substrate.

In the case of multilayer particle arrays, the adhesional deformation may occur in both a bare and an APTMS substrate. However, it was not observed in the bare glass substrate. As shown in Fig. 4b, there were substantial gaps among the particles. The adhesional deformation would not occur in the large gaps or interstices between the particles. This result was closely related to the free-slipping condition, which guarantees a close attachment or dense packing. The adhesional deformation of the hydrated particle by the APTMS-modified surface and the subsequent deformation of the particles within the adsorbed layer provided a template for all subsequent layers to be built on top of this first adsorbed layer to form dense fcc multilayers. In other words, at the very moment that the dense hexagonal layer was formed because of the free-slipping condition, the subsequent layers were fitted onto the pattern of the pre-deformed layer. The strong capillary forces in the middle of the multilayer formation caused the particles in the following layers to deform during natural convection drying. Therefore, packing patterns of the layers separated by several lattice constants from the substrate were

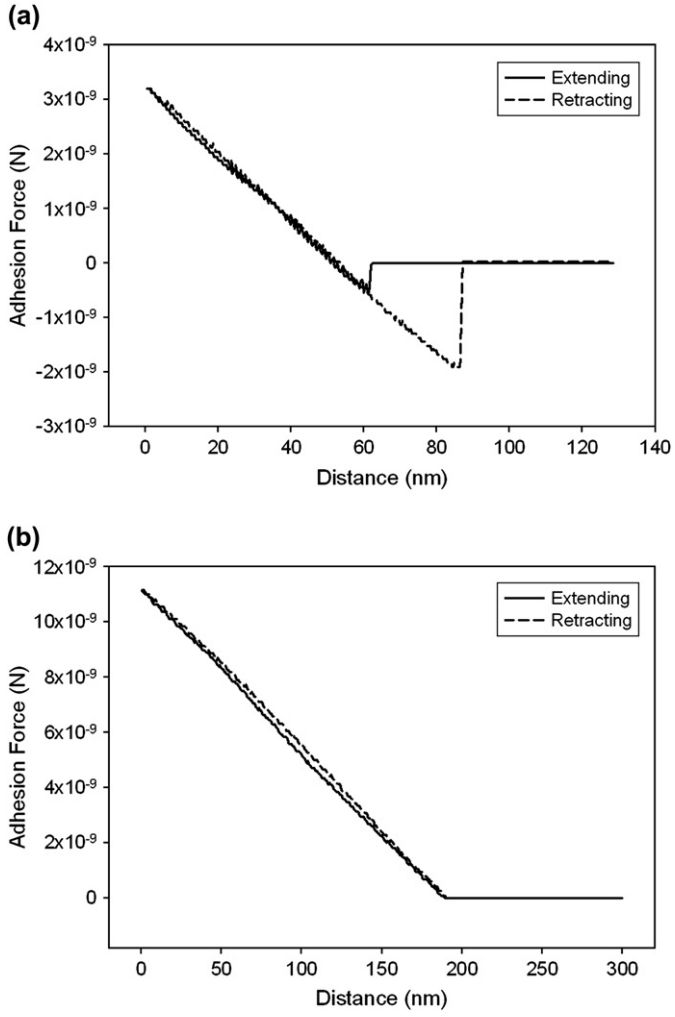

Fig. 5. AFM adhesion force curves: (a) between an SiN_x AFM tip and the surface of poly(St/NaSS) latex particles and (b) between the APTMS-modified SiN_x AFM tip and the surface of poly(St/NaSS) latex particles.

greatly influenced by that of the first layer. The 3-D arrays from the APTMS-modified glass substrate showed a denser packing pattern without crevices (Fig. 4c versus 4f), over a wide area.

In Fig. 6, the FE-SEM micrographs show the cross-section of the 2- and 3-D arrays from the latex particles with various layers on the APTMS-modified glass substrate. The micrographs were captured at the 85° tilt angle. The crystal lattice formed on the APTMS-modified glass substrate showed a honeycomb-like hexagonal packing structure, and so one could see that the dense packing by deformation of the particle shape occurred regardless of the number of crystal layers by 38 layers. A multilayer of the latex particles was believed to be formed instantaneously in one liquid film of variable thickness due to a local variation of the latex concentration with the passage of drying time. In this crystallization cell, the number of layers was mainly determined by the latex concentration on the drying position. Once a nucleus in the cell center was formed, the crystal growth advanced from the ordered array in the cell center toward the cell periphery. The latex particles in the ordered phase attracted the nearest ones and caused a flux directed toward the ordered regions. A monolayer was formed by the mechanism, as shown in Fig. 1b, in the adequately low concentrations of the latex particles around the cell center. At the high concentration of the latex particles around the cell periphery, however, multilayers were easily formed by the intensive convective water flux resulting from the increased local curvature of the liquid layer and the local sucking capillary pressure [5]. In the transition from monolayer to bilayer, square lattices were frequently observed on the bare glass since the square lattice structure had an intermediate thickness ($\sim 1.71 d_o$, where d_o is a particle diameter), which compensated for the liquid meniscus slope, as compared with that ($\sim 1.82 d_o$) of hcp [33,34]. According to the report by Pieranski et al. [34], it has been demonstrated that multilayers can be obtained with the following sequence of layers on the solid glass substrate: $1\Delta-2\square-2\Delta-3\square-3\Delta-\cdots$, as in the case of ours. Here the figures correspond to the number of layers and the symbols mean hexagonal (Δ) or tetragonal ($\square$) packing of the particles. We could observe tetragonal lattices between the hexagonally packed domains in the transition state of layers following the above mentioned sequence of layers. However, an elimination of the square lattices at the top layer couldn't seem to happen in the transition state of layers, as shown in the SEM image of APTMS substrate. In general, the alternating array pattern observed in the transition layers was believed to have originated from the distorted water meniscus between the different layers, and the consequent tetragonal arrays occupied comparatively small widths (usually, 1–5 μm for 200–300 nm particle). On the other hand, square tetragonal array patterns at the center of the topmost multilayer occupied a comparatively wide width (~50 μm). The free-slipping condition made dense packing favorable and resulted in the higher capillary force due to the reduced interstices, which led to hexagonal array patterns in the current work.

Fig. 7 shows the thickness versus the number of layers obtained from the cross-section of the 2- and 3-D particle arrays on the bare and APTMS-modified glass substrates. The average thicknesses of each multilayer were obtained from 5 samples at 4 different points by using an SEM. Fig. 7 demonstrates that the thickness of the particle array with the APTMS substrate was in correlation with the calculated values (solid line) of the 100% hexagonal lattice. On the other hand, the thickness of the bare glass showed explicit deviations from the hexagonal lattice, which indicated the poor packing quality of the particle array. In the case of the APTMS-modified glass substrate, the thickness increased with a proportionality constant of 1.82, which was in good agreement with Eq. (1).

The dependence of the intensity of minimum UV–visible transmission spectra (i.e., stop band) on the crystal thickness was directly determined by measuring the transmission spectra of the crystalline lattices assembled from the latex particles. Fig. 8 shows the transmission spectra recorded at normal incidence to the (111) planes. All samples were dried and the void spaces among the colloids were completely filled

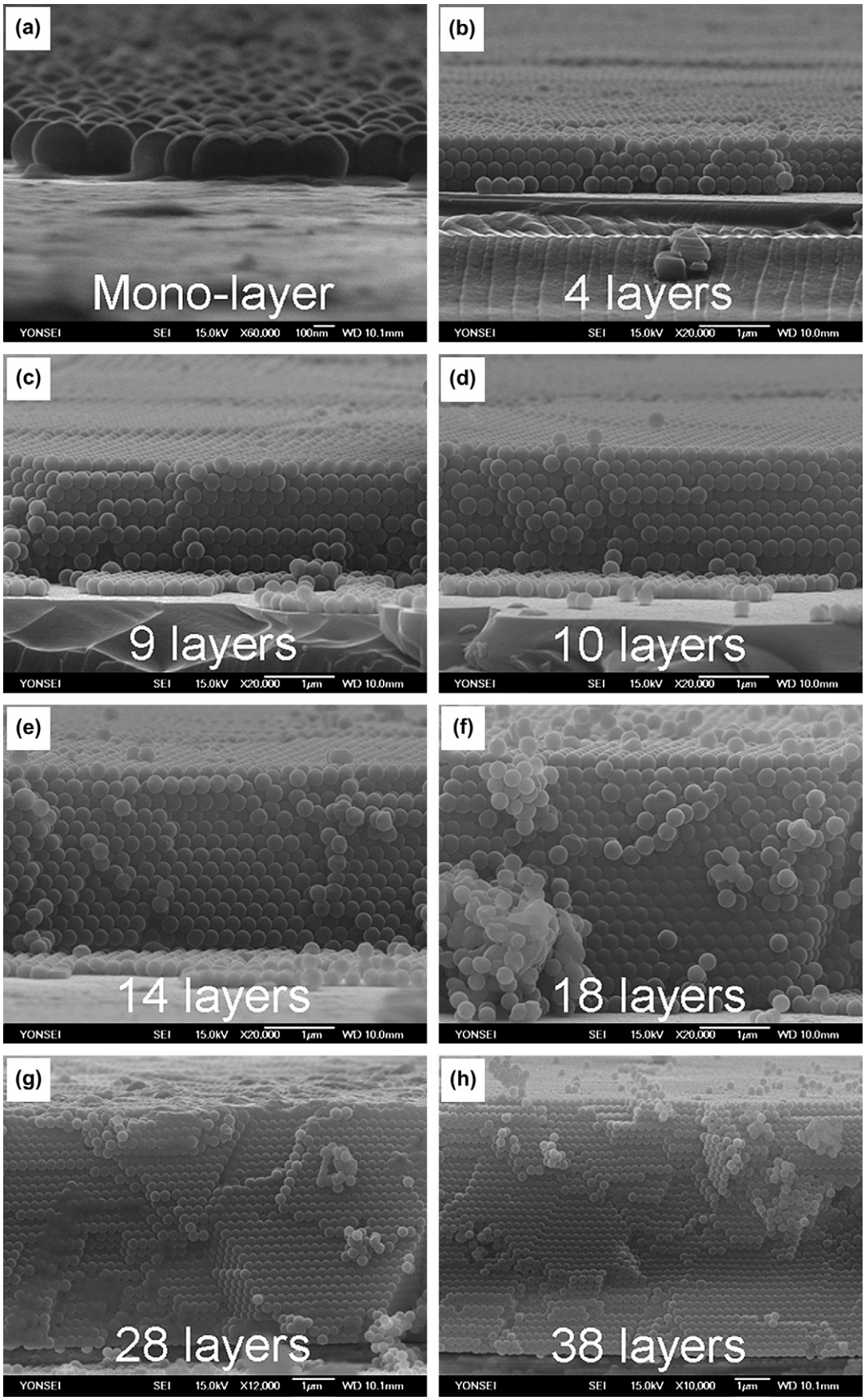

Fig. 6. Cross-sectional SEM images of the 2- and 3-D arrays of the poly(St/NaSS) particles on the APTMS-modified glass substrate, with varying number of layers.

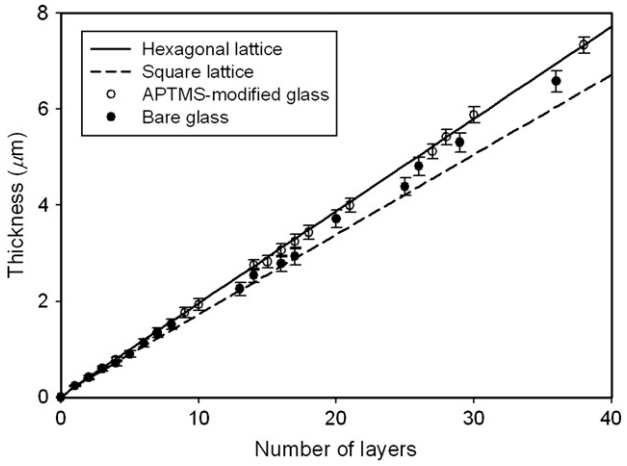

Fig. 7. The thickness of the particle arrays versus the number of layers. The solid (100% hexagonal lattice) and dashed (100% square lattice) lines are calculated values.

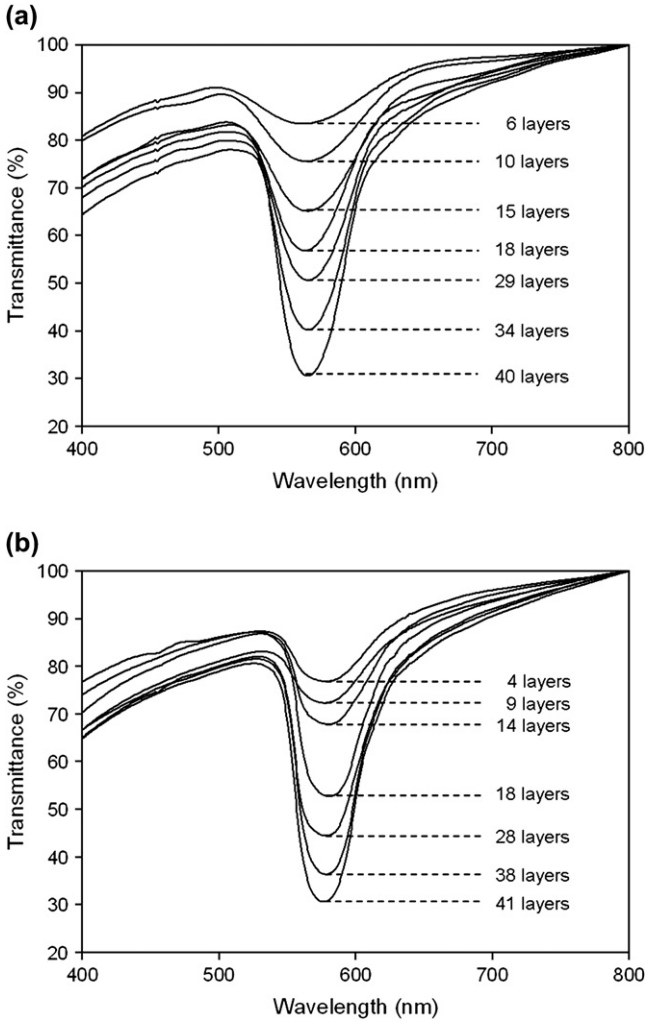

Fig. 8. UV–visible transmission spectra taken at normal incidence to the (111) planes of cubic close-packed lattices (of 234 nm highly charged latex particles) having various thicknesses (a) on the cleaned, bare glass substrate and (b) on the APTMS-modified glass substrate.

with air. The intensity of stop bands was linearly proportional to the crystal thickness when the number of (111) planes increased from 4 to 41 layers on the APTMS-modified glass and from 6 to 40 layers on the cleaned, bare glass. An increase in the intensity of stop bands is a generally known phenomenon, since diffusive light scattering varies with the number of layers of the photonic crystals [35]. The UV beam spot size (1 mm width, 10 mm height, Model: UV-1650PC, Shimadzu) used in the experiment seemed to be larger than that of one crystal (typically $50\times100\ \mu m^2$). Thus, the results in Fig. 6 are the average values measured in the several crystals, whose number of layers was slightly different. The results were in good agreement with the consistent height values (ΔZ) shown in AFM data. In addition, the minimum transmission wavelengths ($\lambda_{T,min}$) were relevant (i.e., the APTMS-modified glass: 579 nm and the bare glass: 565 nm) regardless of the variations of the number of layers. Thus, the results provided statistically significant evidence. It was concluded that a well ordered crystal structure of the particle array on the APMTS-modified substrate could be obtained, since the stop-band width of the APTMS-modified substrate was narrower than that of the bare glass substrate. However, the experimental results did not seem to be narrower than the theoretical values calculated by DLS theory or the Korringa–Kohn–Rostoker (KKR) model [35]. This implies that the results were observed in a polycrystalline colloidal crystal. The APTMS layer prevented 'pinning' of the particle, which was important in reducing point and line defects; however, the simultaneous multi-nucleation was inevitable in the horizontal-type array cells used in the experiment. The simultaneous nuclei formation led to polycrystalline crystals and dislocations.

Fig. 9 shows the surface profile of the outermost multilayer on the (a) bare and (b) APTMS-modified glass substrates in the AFM analysis. From the peak-to-valley profiles in Fig. 9 and the measured values, d or $d_o - d$ in Table 1, it is evident that the particle array on the APTMS-modified glass was more condensed and closely packed, but the deformations in the z-direction (ΔZ) were insignificant (refer Fig. 4a and d). From the optical transmittance data by UV–visible spectrophotometry, the minimum transmission wavelength ($\lambda_{T,min}$) of the colloidal crystal onto the APTMS-modified glass substrate was observed at 579 nm. Suppose that an ideal colloidal crystal is entirely composed of the fcc (or hcp) structure, the $\lambda_{T,min}$ value should be 549 nm calculated using Bragg's diffraction condition: $m\lambda = 2d_{hkl}(n_c^2 - \sin^2\theta)^{1/2}$, where m is an integer, n_c, the refractive index of the crystalline assembly calculated from the interstitial void of hexagonal close packing (0.26) and the reflective indices of air (1.00) and polystyrene (1.59), d_{hkl}, $(2/3)^{0.5}d_o$ (grating constant) for the (111) fcc plane, and the angle of incident light, 0°, respectively [15,36]. This difference between the observed and calculated $\lambda_{T,min}$ probably arose from the value of packing density used. The packing density of the colloid crystals on the APTMS-modified substrate was calculated as 0.80 using Bragg's equation, assuming that the d_{111} for APTMS was the same as the above ideal value, since the ΔZ difference was found to be negligible, as shown in Table 1.

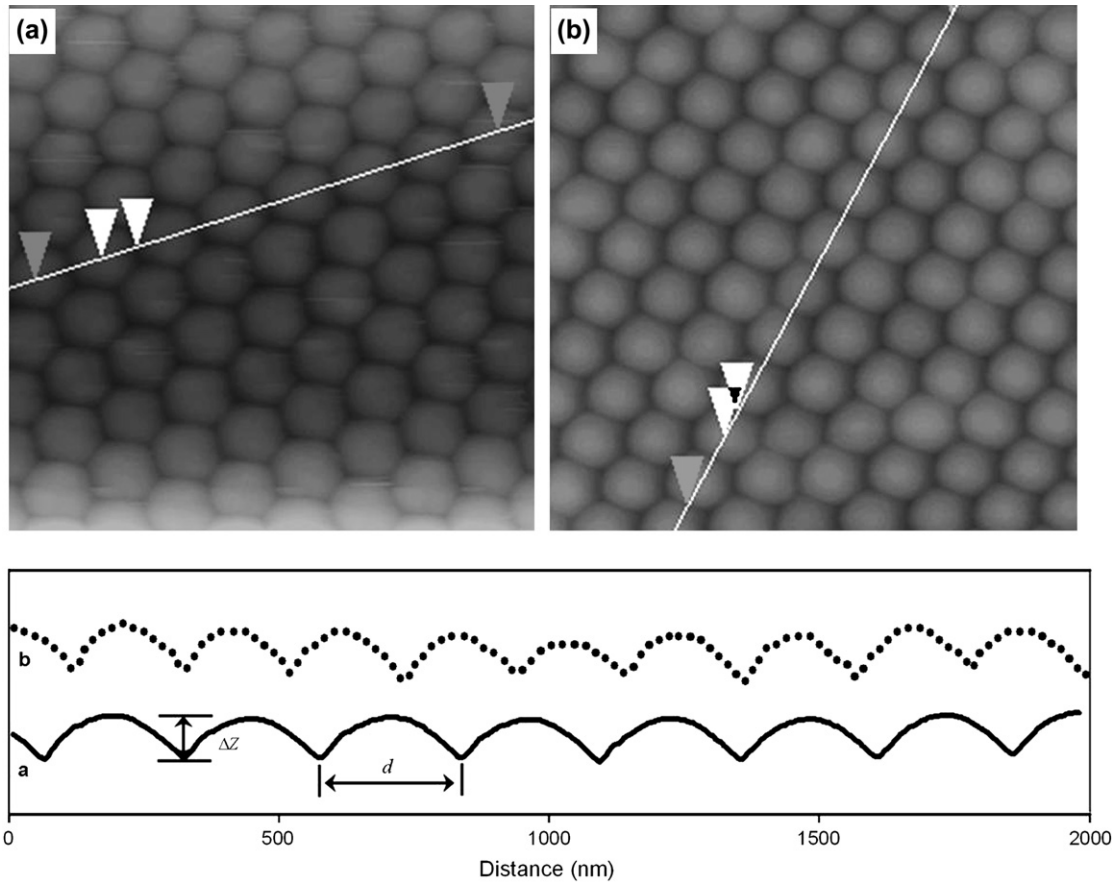

Fig. 9. A tracing of the *z*-axis profiles of the poly(St/NaSS) particle arrays (a) on bare glass and (b) on APTMS-modified glass substrates in the AFM analysis. The nomenclatures for ΔZ and d are given in Table 1.

Table 1
Peak-to-valley data of the cross-sections of the highly charged poly(St/NaSS) particles on (a) bare glass and (b) APTMS-modified glass substrates at 20 °C

Values	*a*	*b*
ΔZ[a]/nm	51 ± 2	53 ± 7
Particles/10^3 nm	3.9	4.8
d[b]/nm	256	209
$d_o - d$[c]/nm	22	−25

[a] Mean peak-to-valley distance.
[b] Interparticle distance calculated from the particle number per 1.0 μm.
[c] The interval between the particles, d_o = original particle diameter. A negative value indicates overlapping morphology due to the deformation.

5. Conclusion

The packing pattern of the highly charged poly(St/NaSS) particles formed on the APTMS-modified glass surface was found to be a square lattice-free hcp structure. This packing pattern can be explained by the nature of APTMS-coated surface which leads to 'free-slipping' of drawing particles into colloid crystal nuclei. The free-slipping condition prevented the in-coming particles from anchoring onto the substrate and made the interstices between particles smaller. Subsequently, a stronger capillary force arising from the smaller interstices caused a substantial particle deformation. The first dense layer served as a template for subsequent multilayer formations on top of it and clearly reduced point and line defects during the multilayer crystal formation to improve packing quality, except for a few dislocations.

Acknowledgement

This work was supported by the Korea Research Foundation Grant funded by the Korean Government (MOEHRD, R08-2003-000-11116-0).

References

[1] Xia Y, Gates B, Yin Y, Lu Y. Adv Mater 2000;12:693–713.
[2] Campbell M, Sharp DN, Harrison MT, Denning RG, Turberfield AJ. Nature 2000;404:53–6.
[3] van Blaaderen A, Rue R, Wiltzius P. Nature 1997;385:321–4.
[4] Egen M, Zentel R. Chem Mater 2002;14:2176–83.
[5] Denkov ND, Velev OD, Kralchevski PA, Ivanov I, Yoshimura H, Nagayama K. Langmuir 1992;8:3183–90.
[6] Dimitrov AS, Dushkin CD, Yoshimura H, Nagayama K. Langmuir 1994; 10:432–40.
[7] Dushkin CD, Lazarov GS, Kotsev SN, Yoshimura H, Nagayama K. J Colloid Polym Sci 1999;277:914–30.
[8] Maenosono S, Dushkin CD, Yamaguchi Y, Nagayama K, Tsuji Y. J Colloid Polym Sci 1999;277:1152–61.

[9] Nagayama K. Phase Transitions 1993;45:185–203.
[10] Yablonovitch E, Gmitter TJ. Phys Rev Lett 1989;63:1950–3.
[11] Ye YH, LeBlanc F, Hache A, Truong VV. Appl Phys Lett 2001;78:52–4.
[12] Zeng F, Sun Z, Wang C, Ren B, Liu X, Tong Z. Langmuir 2002; 18:9116–20.
[13] Jiang P, Hwang KS, Mittleman DM, Bertone JF, Colvin VLJ. J Am Chem Soc 1999;121:11630–7.
[14] Alfrey TJ, Bradford EB, Vanderhoff JW, Oster GJ. J Opt Soc Am 1954;44:603–9.
[15] Goldenberg LM, Wagner J, Stumpe J, Paulke BR, Gornitz E. Mater Sci Eng C 2002;C22:233–7.
[16] Velev OD, Jede TA, Lobo RF, Lenhoff AM. Chem Mater 1998;10:3597–602.
[17] Park SH, Xia Y. Langmuir 1999;15:266–73.
[18] Bevan MA, Lewis JA, Braun PV, Wiltzius P. Langmuir 2004;20:7045–52.
[19] Velev OD, Denkov ND, Paunov VN, Kralchevsky PA, Nagayama K. Langmuir 1993;9:3702–9.
[20] Paunov VN, Kralchevsky PA, Denkov ND, Nagayama K. J Colloid Interface Sci 1993;157:100–12.
[21] Kralchevsky PA, Denkov ND. Curr Opin Colloid Interface Sci 2001; 6:383–401.
[22] Kralchevsky PA, Nagayama K. Langmuir 1994;10:23–36.
[23] Nagayama K. Colloids Surf A 1996;109:363–74.
[24] Dimitrov AS, Nagayama K. Langmuir 1996;12:1303–11.
[25] Cong H, Cao W. Langmuir 2003;19:8177–81.
[26] Im SH, Kim MH, Park OO. Chem Mater 2003;15:1797–802.
[27] Reculusa S, Ravaine S. Chem Mater 2003;15:598–605.
[28] Cheng W, Han X, Wang E, Dong S. Electroanalysis 2004;16:127–31.
[29] Cheong IW, Kim JH. J Colloid Polym Sci 1997;275:736–43.
[30] Cheong IW, Kim JH. Colloids Surf A 1999;153:137–42.
[31] Crocker JC, Grier DG. Phys Rev Lett 1996;77:1897–900.
[32] Herzog CA, Leite CAP, Zaniquelli MED, Galembeck F. Colloids Surf A 1998;144:207–17.
[33] Prevo BG, Velev OD. Langmuir 2004;20:2099–107.
[34] Pieranski P, Strzelecki L, Pansu B. Phys Rev Lett 1983;50:900–3.
[35] Gates B, Lu Y, Li ZY, Xia Y. Appl Phys A 2003;76:509–13.
[36] Cong H, Cao W. Langmuir 2004;20:8049–53.